A Novel Analytical Approach and Finite Element Modelling of a BDFIM

N.H. van der Blij, T.D. Strous, Xuezhou Wang, H. Polinder,

***Abstract* – Nowadays many wind turbines use a doubly fed induction machine (DFIM) as a generator (DFIG). The brushless DFIM (BDFIM), however, has increased fault handling capabilities and suffers less from reliability issues. This paper presents a different method of analytically evaluating the BDFIM. This is done by analyzing the flux density produced by the two stator windings and the interaction with the nested loops of the rotor. Subsequently FEM is used to verify the analytical findings and analyze the behavior of the machine. Additionally several design parameters of the BDFIM such as the pole pair combinations and the number of loops per nest are evaluated. General rules of thumb regarding these design parameters are presented.**

***Index Terms*-- Brushless Double Fed Induction Generator (BDFIG), Brushless Double Fed Induction Machine (BDFIM), Finite Element Modeling (FEM), Nested loop, Torque ripple.**

I. NOMENCLATURE

Physical quantities

A	magnetic vector potential
B	magnetic flux density
p	number of pole pairs
ω	angular frequency or velocity
t	time
τ	pitch length
θ	physical angle along the circumference
φ	electrical angle
i	current
r_r	rotor radius
l_{st}	stack length
λ	flux linkage
L	inductance
R	resistance
T	torque
S	surface/area
η	efficiency
h	harmonic number
C	pole pair combination number
q_r	number of loops per nest

Subscripts and superscripts

p	power winding
c	control winding
r	rotor
s	stator
g	air gap
rl	rotor loop

The research leading to these results has received funding from the European Union's Seventh Framework Programme managed by REA – Research Executive Agency (FP7/2007_2013) under Grant Agreement N.315485.

N.H. van der Blij, T.D. Strous and H. Polinder are with the Department of Electrical Power Processing, Delft University of Technology, Delft, 2628CD The Netherlands (e-mail: n.h.vanderblij@tudelft.nl, t.d.strous@tudelft.nl, x.wang-3@tudelft.nl, h.polinder@tudelft.nl).

II. INTRODUCTION

Wind energy has shown an exponential growth over the past decades and it is anticipated that this growth will continue in the coming years. In 2011 5.3% of the electrical energy consumption in Europe was provided by wind turbines. By 2020, this share is expected to have increased to 12-14% [1].

The common generator topologies for wind turbines are the doubly fed induction machine (DFIM), the squirrel cage induction machine (SCIM), the permanent magnet synchronous machine (PMSM) and the wound rotor synchronous machine (WRSM). Each of these systems has its own strengths and weaknesses [2], [3].

Of the yearly installed power, roughly 50% of the wind turbines have DFIM's. The main advantage of the DFIM is that it works at variable speed with only a fractional power converter that is connected to the rotor via slip rings [4], [5]. The stator winding is directly connected to the grid. However, the DFIM has limited capabilities to handle grid faults and requires slip rings and a gearbox, resulting in reduced reliability and availability [6], [7].

A topology which addresses some of these disadvantages is the brushless DFIM (BDFIM), a machine type in which the brushes are eliminated. Moreover, the BDFIM has the advantage that it generally operates at a lower speed which may imply that one of the gear stages can be omitted. Additionally, the BDFIM has better fault ride-through capabilities [6], [8]-[10].

A BDFIM has two stator windings with different numbers of pole pairs designed in such a way that the stator windings do not couple magnetically. They are sometimes referred to as the power winding and the control winding. The power winding is connected directly to the grid, as the stator winding of a DFIM. The control winding is connected to the grid via a partially rated power electronic converter to enable variable speed, like the rotor winding in a DFIM.

The rotor has to couple to both the stator windings. This is usually done using a nested loop configuration [3], as illustrated in Fig. 1. However, other types, such as the brushless doubly fed reluctance machine (BDFRM), are also possible [11].

Often for the analysis of a BDFIM either analytical equations including harmonics or reluctance networks are used. These methods provide thorough mathematical insight in these machines but do not show the underlying concepts of the BDFIM [8], [12].

In this paper a more fundamental approach is used to show why and how a BDFIM operates. This is done by evaluating the magnetic fields produced by the stator windings and their interaction with the rotor, while space harmonics are neglected.

978-1-4799-4389-0/14/$31.00 ©2014 IEEE

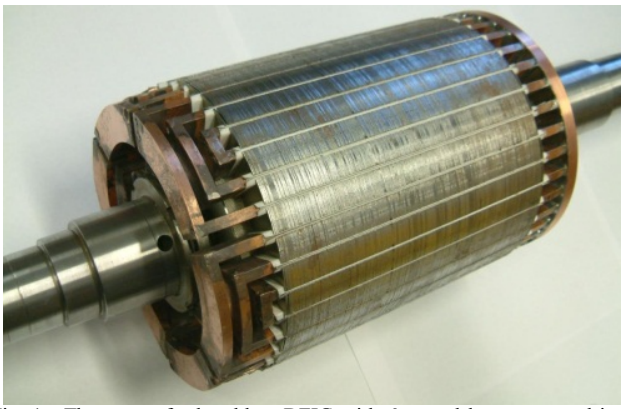

Fig. 1. The rotor of a brushless DFIG with 6 nested loops, as used in a machine with a stator with a 4-pole and an 8-pole winding, reproduced from [3].

Additionally Finite Element Analysis (FEA) is used to assess the influence of several design choices on the power, torque, efficiency and torque ripple of a BDFIM. The design choices that will be considered in this paper are the pole pair combinations and the number of loops per nest.

III. Theoretical Approach

A. Introduction

Understanding the basic operating principles of the BDFIM is different from most AC machine types. The objective of this section is to develop a basic understanding of the torque production based on the magnetic field in the air gap and the induced currents in the nested loops on the rotor. In other words, the question we want to answer in this section is: why does this strange machine with a stator with two stator windings and a rotor with nested loops develop torque?

To answer this question, first the magnetic field in the air gap is analyzed. As in normal AC machines, a stator winding produces a rotating magnetic field in the air gap. However, in this machine, there are two of these stator windings with a different number of pole pairs and designed not to couple magnetically. Therefore, there are two rotating magnetic fields. When these fields are described in the rotor reference frame and added, the combination of these two fields has many characteristics of a standing wave. This is the first important step that is worked out mathematically in the next subsection.

The next question is: how does the rotor with its nested loops interact with this pulsating magnetic field, and why does it develop torque? The answer is basically given by Lenz's law: the rotor is pushed to the position where the change of the flux linkage of the nested loops is minimized. When the machine operates without load, this means that the center of the nested loops coincides with the zero-points of the standing wave, so that the flux linkage of the nested loops is minimized. When a load is applied, the rotor accelerates with respect to the standing waves, and a kind of load angle develops. Therefore, the nested loops move into the pulsating magnetic fields, and currents are induced in the nested loops. The resulting electromagnetic torque that develops pushes the rotor back to the position where the flux linkage of the rotor loops is minimum. This is the second important step that is worked out mathematically in further subsections.

In a comparable way, it could be shown that the rotor poles of a brushless doubly fed reluctance machine (BDFRM) have a tendency to align with the pulsating magnetic field. However, this is not further discussed in this paper.

B. Magnetic flux density in the air gap

As said, the BDFIM has two stator windings, the power winding and the control winding. Each winding has its own number of pole pairs (p_p and p_c) and frequency (ω_p and ω_c). Balanced three-phase windings are assumed and space harmonics are neglected. Balanced sets of three-phase currents are assumed and time harmonics are neglected. The magnetic flux density in the air gap produced by these windings B_g as a function of time t and as a function of the angle along the stator circumference θ_s is then given by

$$B_{gp} = \hat{B}_{gp}\cos(\omega_p t + p_p\theta_s + \varphi_p) \tag{1}$$

$$B_{gc} = \hat{B}_{gc}\cos(\omega_c t + p_c\theta_s + \varphi_c) \tag{2}$$

It is beneficial to convert them to the the rotor connected coordinate system using

$$\theta_s = \theta_r - \omega_m t \tag{3}$$

where ω_m is the angular velocity of the rotor and θ_r is the angle along the rotor circumference.

The resulting flux densities are given by

$$B_{gp} = \hat{B}_{gp}\cos((\omega_p - p_p\omega_m)t + p_p\theta_r + \varphi_p) \tag{4}$$

$$B_{gc} = \hat{B}_{gc}\cos((\omega_c - p_c\omega_m)t + p_c\theta_r + \varphi_c) \tag{5}$$

The derivations can be simplified by substituting an appropriate value for the rotor angular velocity ω_m. Such a value can be determined from (4) and (5), which show that the frequencies of the rotor quantities are given by

$$\begin{aligned}\omega_{rp} &= |\omega_p - p_p\omega_m| = |p_p\omega_m - \omega_p| \\ \omega_{rc} &= |\omega_c - p_c\omega_m| = |p_c\omega_m - \omega_c|\end{aligned} \tag{6}$$

If the machine has to produce a constant torque, the quantities in the rotor must have the same frequency. Therefore, both flux density components must have the same frequency. This exclusively occurs when $\omega_{rp}=\omega_{rc}$. This condition is met if the angular velocity of the rotor ω_m is given by

$$\omega_m = \frac{\omega_p + \omega_c}{p_p + p_c} \qquad \left(\text{or} \quad \omega_m = \frac{\omega_p - \omega_c}{p_p - p_c}\right) \tag{7}$$

The first operating point is used, which implies that the frequency of the electric quantities in the rotor is given by

$$\omega_r = \frac{p_c\omega_p - p_p\omega_c}{p_p + p_c} \tag{8}$$

The rotor angular velocity given in (7) is often called the synchronous speed. Substitution of (7) into (4) and (5) results in

$$B_{gp} = \hat{B}_{gp}\cos(\omega_r t + p_p\theta_r + \varphi_p) \tag{9}$$

$$B_{gc} = \hat{B}_{gc}\cos(-\omega_r t + p_c\theta_r + \varphi_c) \tag{10}$$

The two flux densities are added to achieve the total air gap flux density due to the stator B_{gs}. For the ease of computation it is assumed that $\hat{B}_{gp} = \hat{B}_{gc} = \hat{B}_g$. The air gap flux density due to both stator windings can then be written as

$$B_{gs} = 2\hat{B}_g \cos\left(\frac{p_p + p_c}{2}\theta_r + \frac{\varphi_p + \varphi_c}{2}\right) \cdot \cos\left(\omega_r t + \frac{p_p - p_c}{2}\theta_r + \frac{\varphi_p - \varphi_c}{2}\right) \quad (11)$$

This equation shows what the previous subsection called the first important step of the analysis. It shows that the air gap flux density in the rotor reference frame has many characteristics of a standing wave. This standing wave has frequency ω_r and (p_p+p_c) poles. Additionally, the phase difference in time is distributed along the rotor circumference with (p_p-p_c) poles. Fig. 2 depicts an example of such a flux density.

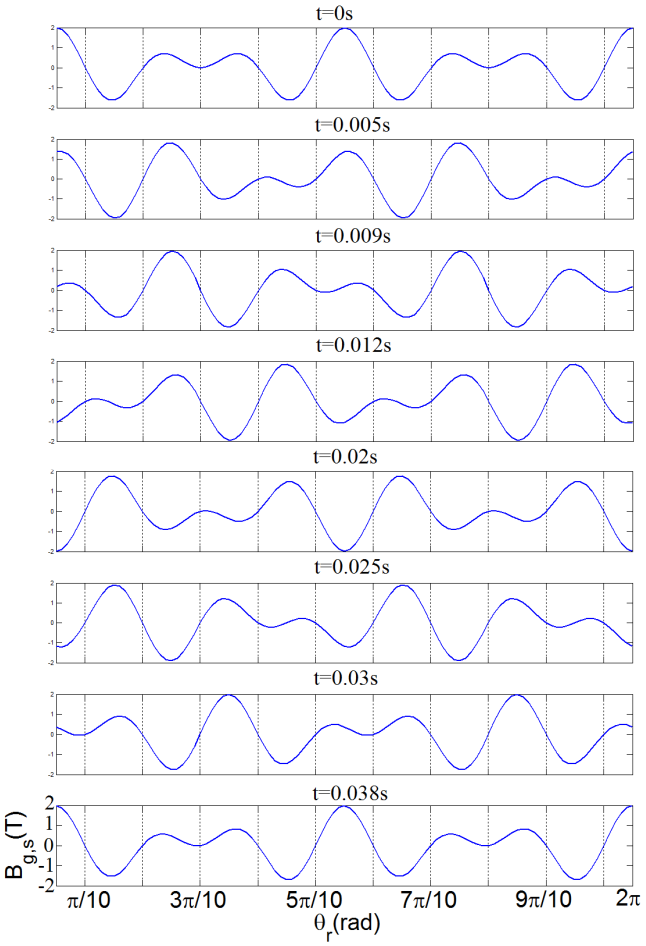

Fig. 2. Flux density distribution for a BDFIM with 6 and 4 pole pairs.

C. *Flux linkage of the rotor*

As derived in the previous subsection, the magnetic flux density distribution behaves as a (p_p+p_c) pole system. This flux density is optimally coupled by a rotor configuration that has the same number of poles. A commonly used rotor configuration has (p_p+p_c) nests consisting of nested loops. In the example of Fig. 1, the rotor has 6 nested loops because the stator windings have 2 and 4 pole pairs (4 and 8 poles).

For the analysis in this paper, a simple rotor structure of (p_p+p_c) nests with one short-circuited loop is chosen. For now it is assumed this loop envelops its full pitch τ:

$$\tau = \frac{2\pi}{p_p + p_c} \quad (12)$$

To determine the flux linkage of one rotor loop λ_{rl}, (9) and (10) should be integrated over the loop pitch τ:

$$\lambda_{rl} = r_r l_{st} \int_{\theta_0}^{\theta_0+\tau} (B_{gp} + B_{gc}) \mathrm{d}\theta_r \quad (13)$$

where θ_0 is the arbitrarily chosen position of one of the conductors of the loop on the rotor circumference (θ_r).

Equation (13) shows that the flux linkage of the rotor loop consists of two parts, a part due to the power winding and a part due to the control winding. The resulting integrals can be worked out to

$$\lambda_{rlp} = \hat{\lambda}_p \cos(\omega_r t + \frac{p_p \tau}{2} + p_p\theta_0 + \varphi_p) \quad (14)$$

$$\hat{\lambda}_p = \frac{2r_r l_{st}}{p_p}\hat{B}_g \sin\left(\frac{p_p \pi}{p_p + p_c}\right)$$

$$\lambda_{rlc} = \hat{\lambda}'_c \cos(\omega_r t - \frac{p_c \tau}{2} - p_c\theta_0 - \varphi_c) \quad (15)$$

$$\hat{\lambda}'_c = \frac{2r_r l_{st}}{p_c}\hat{B}_g \sin\left(\frac{p_c \pi}{p_p + p_c}\right)$$

The amplitudes of these flux linkages have opposite signs because one of the arguments of the sine in the amplitudes of (14) and (15) is smaller than $\pi/2$, while the other argument is larger than $\pi/2$. To give both amplitudes the same sign, a minus sign is added to the expression for the amplitude in (15) and π is added to the argument of the cosine. The resulting flux linkage is given by

$$\lambda_{rlc} = \hat{\lambda}_c \cos(\omega_r t - \frac{p_c \tau}{2} - p_c\theta_0 - \varphi_c + \pi) \quad (16)$$

$$\hat{\lambda}_c = -\frac{2r_r l_{st}}{p_c}\hat{B}_g \sin\left(\frac{p_c \pi}{p_p + p_c}\right)$$

Because the flux linkage of the rotor loops from both stator windings has a frequency of ω_r they can be combined into a single cosine:

$$\lambda_{rl} = \hat{\lambda}_{rl} \cos(\omega_r t + \varphi_\lambda) \quad (17)$$

where

$$\hat{\lambda}_{rl} = \sqrt{\hat{\lambda}_p^2 + \hat{\lambda}_c^2 - 2\hat{\lambda}_p\hat{\lambda}_c \cos(\delta)} \quad (18)$$

$$\delta = \left(\frac{p_p \tau}{2} + p_p\theta_0 + \varphi_p\right) - \left(-\frac{p_c \tau}{2} - p_c\theta_0 - \varphi_c + \pi\right) \quad (19)$$

$$= (p_p + p_c)\theta_0 + \varphi_p + \varphi_c$$

φ_λ is not of importance in this paper.

These equations show that the machine behavior is dependent on the position of the rotor loop in relation to the magnetic flux density distribution in the air gap. Two interesting conclusions can be drawn from (17), (18) and (19).

- It is only possible to operate this machine without any rotor current when the amplitudes of λ_p and λ_c are equal.
- The flux linkage and thus the current in the rotor can be controlled using either the rotor position (θ_0) or the angles of the stator flux density distributions (φ_p and φ_c).

The second conclusion implies that we could choose the angles of the stator flux density distributions (φ_p and φ_c) to be zero, so that the performance of the machine is purely determined by the position of the nested loops on the rotor. In this case, (11) can be written as

$$B_{gs} = 2\hat{B}_g \cos\left(\frac{p_p + p_c}{2}\theta_r\right)\cos\left(\omega_r t + \frac{p_p - p_c}{2}\theta_r\right) \quad (20)$$

and (19) can be written as

$$\delta = (p_p + p_c)\theta_0 \tag{21}$$

D. Torque production

To determine the torque produced by this machine, first the current induced in the rotor loop is determined. The effect of the rotor current on the air gap flux density is in this first approximation assumed to be negligible. This assumption makes sense if the stator windings are connected to voltage sources, because they keep the flux linkage of the stator windings constant. Currents in the rotor are compensated by additional currents in the stator. For the power winding, this is normally the case. For the control winding, this depends on the control.

The amplitude of the current in the rotor loop i_{rl} can be calculated as

$$\hat{i}_{rl} = \frac{\omega_r \hat{\lambda}_{rl}}{\sqrt{R_{rl}^2 + \omega_r^2 L_{rl}^2}} \tag{22}$$

The rotor frequency ω_r is typically between 25% and 75% of the power winding frequency ω_p. Therefore, the resistance term in this equation is expected to be negligible compared to the inductance term. As a result, the amplitude of the current is proportional to the flux linkage and the current is in phase with the flux linkage, while the current has such a direction that the flux it produces opposes the stator flux. This implies the rotor current can be written as

$$i_{rl} = \frac{\hat{\lambda}_{rl}\cos(\omega_r t + \varphi_\lambda)}{L_{rl}} \tag{23}$$

The torque on one rotor loop can be approximated by

$$T_{rl} \propto i_{rl} B_{gs}(\theta_0) - i_{rl} B_{gs}(\theta_0 + \tau) \approx 2 i_{rl} B_{gs}(\theta_0) \tag{24}$$

In this equation, the first cosine term of (20) is used to express the flux density as a function of θ_0. According to (18), the current is proportional to the flux linkage. The relation between θ_0 and δ is given by (21). If this is all substituted in (24), the result is

$$T_{rl} \propto \cos\left(\frac{\delta}{2}\right)\sqrt{\hat{\lambda}_p^2 + \hat{\lambda}_c^2 - 2\hat{\lambda}_p\hat{\lambda}_c\cos(\delta)} \tag{25}$$

In case the amplitudes of λ_p and λ_c are equal, this equation reduces to

$$T_{rl} \propto \cos\left(\frac{\delta}{2}\right)\sin(\delta) \tag{26}$$

Apparently, δ can be seen as a kind of load angle.

If one side of the loop is chosen to be on the point where the flux density is maximum (θ_0=0, δ=0), the flux linkage and the rotor current are minimum, as appears from (18) This appears to be a point where the torque is zero.

If one side of the loop is at $\theta_0=\tau/4$ (so $\delta=\pi/2$), the rotor loop has a significant flux linkage (18) and therefore a significant current. At the location of the conductors of the rotor loop, there is also a significant flux density (20). Both current and flux density vary cosinusoidally with approximately the same phase. The resulting torque (25) tries to push the rotor loops back to the position with minimum flux linkage.

If one side of the loop is chosen at such a position that the flux linkage and the rotor current are maximum, ($\theta_0=\tau/2$, $\delta=\pi$, see (18)), the flux density (20) at these locations is zero. This is again an operating point where the torque is zero, as appears from (25).

This concludes the second part of this analysis intended to show that the rotor nests are pushed to the position where the flux linkage of the rotor loops is minimum. In this position, the center of the nested loops coincides with the zero-points of the standing wave, so that the flux linkage of the nested loops is minimized.

IV. Finite Element Analysis

A 2D FE model was developed to analyze the steady state behavior and the design of a BDFIM. First some aspects of the FE model will be discussed. Subsequently the behavior and some design parameters of the machine are analyzed.

A. Finite Element model

The FE model was developed using Matlab and Comsol Multiphysics. Matlab is used to create an arbitrary machine geometry in Comsol from several input variables. Subsequently the model is run and information such as power, losses and efficiency is extracted. In this way the model can also be used for optimization purposes.

As input for the stator windings either current or voltage sources can be used. In this case current sources are chosen because for the following analyses it is sufficient to operate the machines at nominal current.

For the rotor loop currents Kirchhoff's voltage law is used to derive an equation. This equation is added to the system equations of the FE model. The equation for a rotor loop is given by

$$\frac{l_{st}}{S_{rl}}\frac{\mathrm{d}\iint A\,\mathrm{d}S_{rl+} - \iint A\,\mathrm{d}S_{rl-}}{\mathrm{d}t} + I_{rl}R_{rl} = 0 \tag{27}$$

where A is the magnetic vector potential, and S_{rl+} and S_{rl-} are the surface of the go conductor and the return conductor respectively.

The first term accounts for self-inductance and the mutual inductance of the rotor loop. The second term accounts for the resistance drop over the rotor loop.

For the analysis a machine is used which main parameters are given in Table I. Additionally, the geometry of this machine is shown in Fig. 3.

An example of the obtained distribution of the flux density and the flux lines are shown in Fig. 4 and Fig. 5.

Fig. 6 depicts a comparison of the air gap flux density due to the stator currents obtained from analytical and finite element calculations. Because of the stator and rotor slots, finite element calculations include more harmonics. However, the trend is very much comparable.

TABLE I
MAIN BDFIM PARAMETERS FOR THE ANALYZED MACHINE

Machine parameter	
Stator outer diameter	1.66 m
Stator inner diameter	1.34 m
Stack length	1.60 m
Pole pairs (power, control)	4 , 6
Loops per nest	1
Rated speed	360 rpm
Rated power	3.0 MW

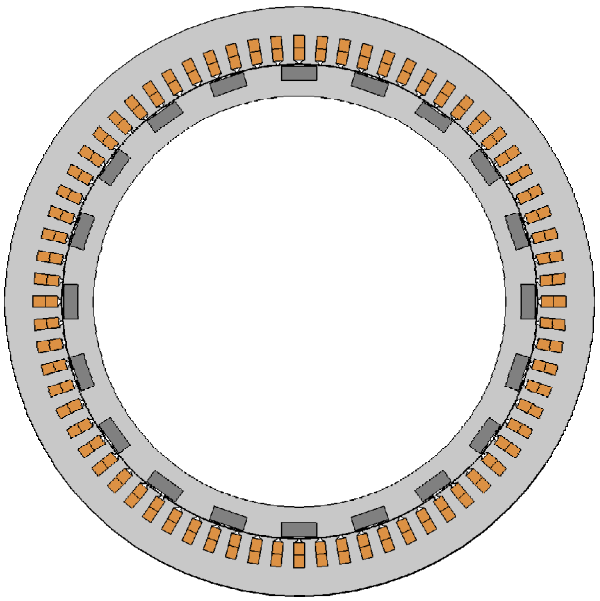

Fig. 3. Geometry of the analyzed BDFIM.

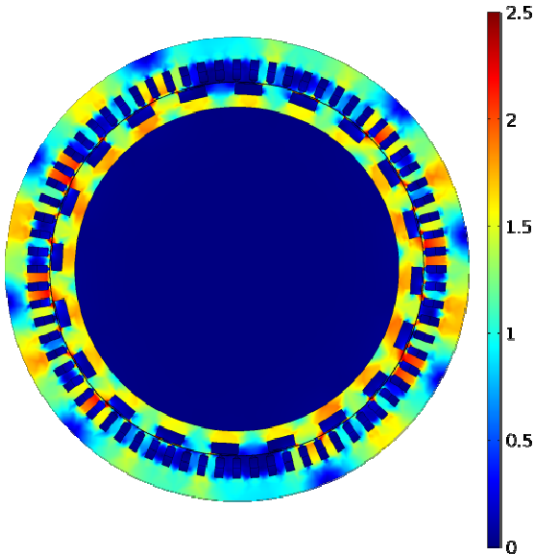

Fig. 4. 2D Patterns of flux densities of the analyzed BDFIM.

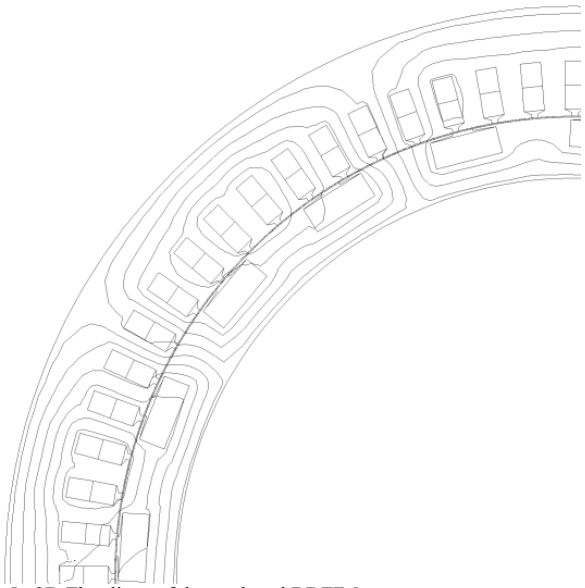

Fig. 5. 2D Flux lines of the analyzed BDFIM.

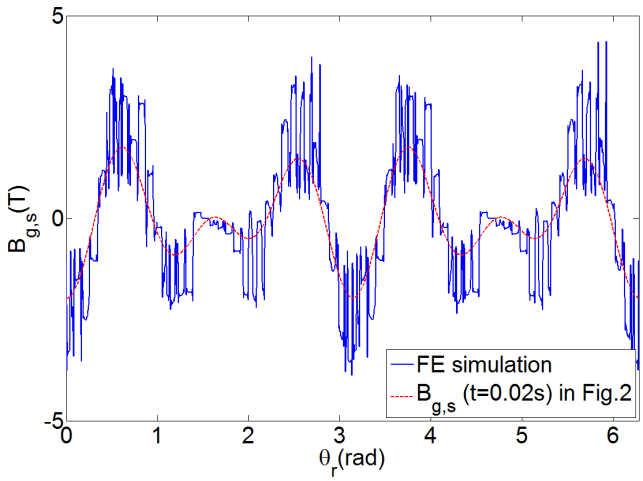

Fig. 6. Comparison of an analytical and a finite element calculation of the radial components of the air gap flux density due to the stator currents.

B. Performance as a function of rotor position

The previous section showed that the rotor current and the torque (and thus the power) of a BDFIM is strongly dependent on the position of rotor relative to the magnetic field of the stator.

In this subsection, FEM is used to confirm this behavior. The machine presented in the previous subsection will be evaluated for several θ_0. The power, efficiency and rotor current as function of θ_0 are shown in Fig. 7.

Fig. 7 shows that the behavior inferred in the previous section is correct. The power is dependent on the position of the rotor. The relation between the position and the power strongly correlates with the behavior of a synchronous machine. However the relation is not a perfect sinusoid. This is consistent with the previous section.

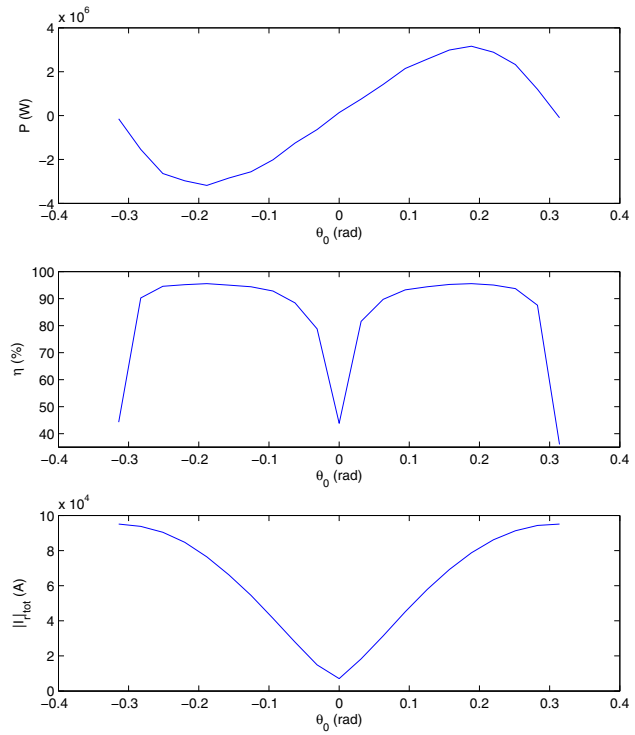

Fig. 7. Power, efficiency and total rotor current as function of θ_0.

The current in the rotor is also dependent on the position of the rotor and it is shown that there is no angle θ_0 where the rotor current is zero. This confirms the behavior derived in (18), (22) and (25).

Additionally the efficiency of the machine was determined. For this machine the maximum efficiency occurs at the point of maximum torque. However this may not be the case for all BDFIM's as copper and iron losses are strongly dependent on the geometry and one might dominate the other. If conductor losses are dominant the maximum efficiency might shift towards θ_0=0 (so δ=0), where if iron losses are dominant it might shift towards other operating points.

C. Pole pair combinations

In [13] it is discussed that the stator windings do not couple if they do not have any harmonics in common. The set of harmonics the two three-phase windings produce is given by

$$h_p = p_p(2t-1), \quad t \in \mathbb{N}^+ \tag{28}$$

$$h_c = p_c(2t-1), \quad t \in \mathbb{N}^+ \tag{29}$$

A pole pair is then suitable if and only if $h_p \cap h_p = 0$. A simple script is used to determine suitable pole pair combinations.

Furthermore, the resultant flux density waveform of (20) is strongly asymmetric. An asymmetric waveform can cause an unbalanced magnetic pull. To ensure that there is no unbalanced magnetic pull the resultant waveform must have a periodicity along the rotor circumference that is higher than one. In other words the waveform must repeat itself from θ_r=0 to θ_r=2π.

This is the case if and only if the greatest common divider of p_p and p_c is not one. This is because the power winding and the control winding have a periodicity of p_p and p_c respectively (see (1) and (2)).

The subset of pole pair combinations (up to 10 pole pairs) that do not couple and do not produce an unbalanced magnetic pull is shown in Table II. For all pole pair combinations shown in Table II the power, torque, torque ripple and efficiency are calculated. The results are shown in Fig. 8.

From Fig. 8 it can be deduced that numbers of pole pairs that are doubles of each other produce high torque ripples compared to other pole pair combinations. This may be caused by harmonics coupling via the rotor. Furthermore, it can be seen that a higher number of poles generally produces a higher torque.

The pole pair combination that is found the best suited is 6 and 4. This combination has relatively high power, torque and efficiency and has relatively low torque ripple.

TABLE II
POLE PAIR COMBINATIONS THAT DO NOT COUPLE OR PRODUCE UNBALANCED MAGNETIC PULL

Combination number (C)		
1	2	4
2	2	8
3	3	6
4	4	6
5	4	8
6	4	10
7	5	10
8	6	8
9	6	9
10	8	10

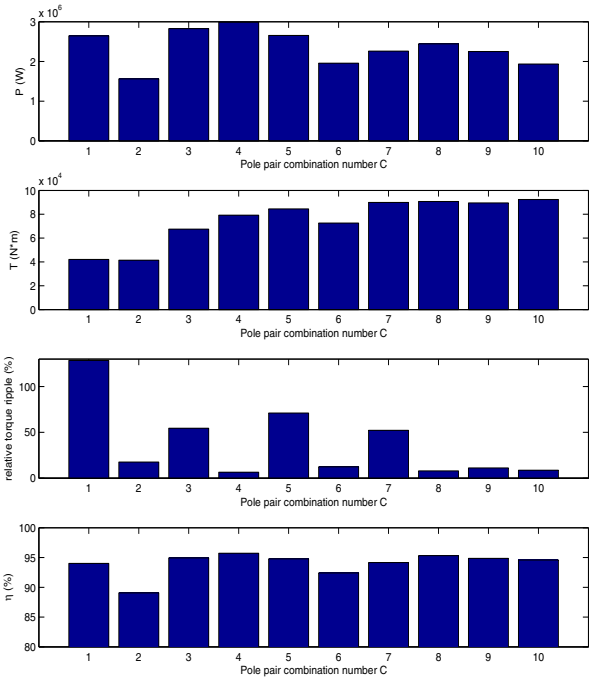

Fig. 8. Power, torque, torque ripple, efficiency for the various pole pair combinations.

D. Loops per nest

Lastly the number of loops per nest will be evaluated when the rotor slots are evenly distributed. In Fig. 9, the power, torque, torque ripple and efficiency are evaluated for several numbers of loops per nest. In theory a higher number of loops would reduce the space harmonic content of the rotor and therefore reduce the torque ripple. Fig. 9 shows that the higher the number of loops per nest in the machine the higher the power and efficiency are. However, the manufacturing cost will somewhat increase and there are numbers of loops per nest that couple more harmonics and increase torque ripple. A suitable number of loops per nest for this case study is found to be five.

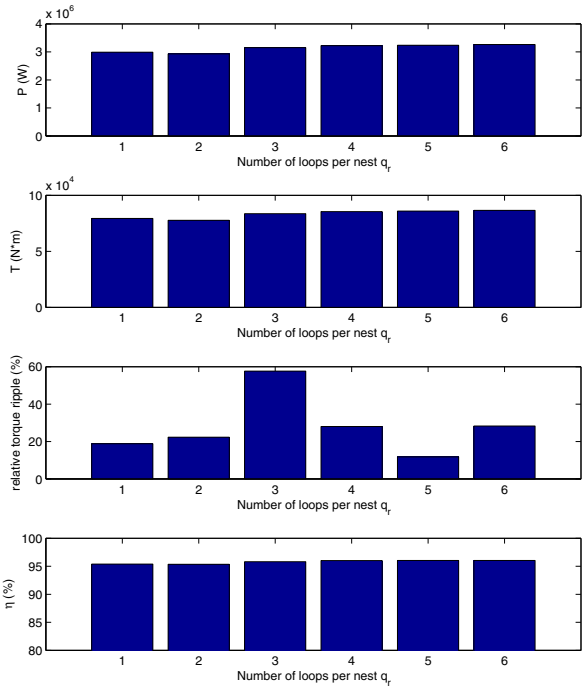

Fig. 9. Power, torque, torque ripple and efficiency for various loops per nest.

V. CONCLUSIONS

A novel method of analytically analyzing the behavior of a BDFIM has been described. The equations show that the rotor current and the torque are strongly dependent on the position of the rotor relative to the stator magnetic flux density. Consequently the operating point of the machine can be regulated using the rotor position and/or stator phase shifts.

A 2D FE model confirms the behavior and analyzes some design parameters. Rules of thumb are presented for picking a suitable pole pair combination and the number of loops per nest. For the presented machine, 4 and 6 poles is the most suitable combination and the number of loops per nest is most favorable at 5.

This paper gives insight into the BDFIM from a different point of view and into some of the design parameters. However further work needs to be done to generalize the findings and to analyze the remaining design parameters of the BDFIM.

VI. REFERENCES

[1] G. Shrestha, “Structural flexibility of large direct drive generators for wind turbines”, PhD dissertation, Delft University of Technology, Netherlands, 2013.

[2] H. Polinder, "Overview of and trends in wind turbine generator systems" *Proceedings of the IEEE Power and Energy Society General Meeting*, pp. 1-8, 24-29 July 2011.

[3] H. Polinder, J.A. Ferreira, B.B. Jensen, A.B. Abrahamsen, K. Atallah, R.A. McMahon, "Trends in wind turbine generator systems," *IEEE Journal of Emerging and Selected Topics in Power Electronics*, vol.1, no.3, pp. 174-185, Sept. 2013.

[4] M. Liserre, R. Cardenas, M. Molinas, J. Rodriguez, "Overview of multi-MW wind turbines and wind parks," *IEEE Transactions on Industrial Electronics*, vol.58, no.4, pp.1081,1095, April 2011.

[5] H. Li, Z. Chen, "Overview of different wind generator systems and their comparisons," *IET Renewable Power Generation*, vol.2, no.2, pp. 123-138, June 2008.

[6] I. Azmy, A. Abdel-Khalik, A.M. Massoud, Ahmed Shehab, "Assessment of fault-ride through capability of grid-connected brushless DFIG wind turbines," *IET Conference on Renewable Power Generation (RPG 2011)*, pp. 1-7, 6-8 Sept. 2011.

[7] S. Tohidi, H. Oraee, M. R. Zolghadri, S. Shao, P. Tavner, "Analysis and enhancement of low-voltage ride-through capability of brushless doubly fed induction generator," *IEEE Transactions on Industrial Electronics*, vol.60, no.3, pp. 1146-1155, March 2013.

[8] H. Gorginpour, H. Oraee, R. A. McMahon, "Electromagnetic-thermal design optimization of the brushless doubly fed induction generator," *IEEE Transactions on Industrial Electronics*, vol.61, no.4, pp. 1710-1721, April 2014.

[9] S. Shao, T. Long, E. Abdi, R. A. McMahon, Y. Wu, "Symmetrical low voltage ride-through of the brushless doubly-fed induction generator," *37th Annual Conference on IEEE Industrial Electronics Society IECON 2011*, pp. 3209-3214, 7-10 Nov. 2011.

[10] T. Long, S. Shao, E. Abdi, R.A. McMahon, S. Liu, "Asymmetrical low-voltage ride through of brushless doubly fed induction generators for the wind power generation," *IEEE Transactions on Energy Conversion*, vol.28, no.3, pp. 502-511, Sept. 2013.

[11] R.A. McMahon, P. Tavner, E. Abdi, P. Malliband, D. Barker, "Characterising rotors for brushless doubly-fed machines (BDFM)," *XIX International Conference on Electrical Machines (ICEM)*, pp. 1-6, 6-8 Sept. 2010

[12] H. Gorginpour, H. Oraee, R.A. McMahon, "A novel modeling approach for design studies of brushless doubly fed induction generator based on magnetic equivalent circuit," *IEEE Transactions on Energy Conversion*, vol.28, no.4, pp. 902-912, Dec. 2013.

[13] P.C. Roberts, “A study of brushless doubly-fed (induction) machines”, PhD dissertation, University of Cambridge, 2005.

VII. BIOGRAPHIES

Nils Hans van der Blij was born in Leiden in the Netherlands, on March 11, 1990. He graduated bachelors and masters from the Technical University of Delft in 2011 and 2013 respectively.

His employment experience included Scarabee, Philips, and Delft University of Technology. His special fields of interest are electrical machines and drives and sustainable energy generation.

Tim D. Strous received the MSc degree in electrical engineering from Delft University of Technology, Delft, The Netherlands, in 2010.

Currently he is working towards the Ph.D. degree in the field of electrical machines. His current research interests include modeling and design of electrical machines.

Xuezhou Wang received the MSc in electrical engineering from Northwestern Polytechnical University, Xi’an, China, in 2012.

Currently he is working towards his PhD degree in the field of electrical machines. His current research interests include numerical modeling and design of electrical machines.

Henk Polinder received the MSc and the PhD degree from Delft University of Technology, Delft, The Netherlands, in 1992 and 1998. Since 1996 he has been an assistant/associate professor in the Electrical Power Processing Group of Delft University of Technology.

He worked part-time at Lagerwey in Barneveld in 1998/1999, at Philips Applied Technologies in Eindhoven in 2002 and at ABB Corporate Research in Vasteras in 2008. He was a visiting professor at the University of Newcastle-upon-Tyne in 2002, at Laval University, Quebec in 2004 and at the University of Edinburgh in 2006.

He is author or co-author of over 200 papers. His research interests include design aspects of electrical machines, mainly for renewable energy applications.